Microstructural evolution of tungsten under thermal loads: A comparative study between cyclic high heat flux loading and isochronous furnace heating

Narguess Nemati [a,b,*], A. Manhard [a], H. Greuner [a], K. Hunger [a], B. Böswirth [a], E. Visca [c], J.H. You [a]

[a] Max Planck Institute for Plasma Physics, Boltzmannstr. 2, 85748 Garching, Germany
[b] Surface Mechanics and Tribology group, Department of Mechanical and Production Engineering, Aarhus University, Inge Lehmanns Gade 10, Navitas, 8000 Aarhus C, Denmark
[c] ENEA, Department of Fusion and Technology for Nuclear Safety and Security, Frascati, Italy

ARTICLE INFO

ABSTRACT

Recrystallization is one of the most pronounced microstructural changes of tungsten when subjected to cyclic high heat flux (HHF) loads. In the framework of the European DEMO divertor development an intensive R&D programme is being performed. Many HHF tests of tungsten monoblocks have shown that recrystallization and grain growth have been deemed a major degradation feature leading to brittleness and reduced strength. In the previous recrystallization studies, tungsten was normally heat-treated in a furnace in slow uniform heating. However, in a HHF test or in the assumed fusion reactor operation, the water-cooled tungsten armor is rapidly heated by cyclic HHF pulses generating a steep temperature gradient (20 MW/m^2 loading results in about 200 K/mm) and thermal stresses. This difference raises the question as to whether a furnace heat-treatment condition properly simulates the cyclic HHF loading case in terms of recrystallization behaviour if the heat exposure conditions are kept comparable to each other. The present paper addresses this issue. To this end, a comparative microstructural study was performed for two different groups of tungsten samples: one tested under well-defined furnace heat-treatment conditions (1500 °C, 2100 °C) and the other one taken from the monoblocks (at the positions of the same corresponding temperatures) of a water-cooled mock-up tested under HHF loads at 20 MW/m^2, 500 cycles. Extensive quantitative image analysis was carried out based on detailed microstructural and crystallographic characterization and micro-hardness was measured. The HHF loaded surface is dominated by the formation of extremely large grains in contrast to furnace heating at the same temperature. The samples heated at 2100 °C exhibited a remarkable difference in recrystallization and grain growth behaviour and hardness values between the two heating cases. Two commercial tungsten grades (AT&M, ALMT) showed a similar behaviour to each other.

1. Introduction

The divertor target plates are the most severely loaded components in a fusion reactor [1]. The severe loads, generated by high-heat-fluxes (HHF) due to intense plasma particle bombardment affect the armor material (tungsten) of the plasma facing components (PFCs) and causing detrimental microstructural changes such as recrystallization and grain growth. A recent HHF testing campaign conducted on many water-cooled tungsten monoblock target mock-ups revealed that extensive recrystallization occurred in the upper part of the tungsten blocks where

temperature was higher than 1200 °C. The near surface region of the tungsten armor underwent significant grain growth if the temperature exceeded 2000 °C. Such permanent microstructural changes affect the mechanical properties of the armor material and may reduce the operational performance of the PFCs. Recrystallization in tungsten has been shown to promote brittleness at low temperatures and reduce yield strength at high temperatures compared to the as-produced (highly deformed) state. The recrystallization-induced brittleness (commonly referred to as recrystallization embrittlement [2]) has been quantified in terms of reduction in total elongation [3], bending stress [4], fracture

---

toughness [5,6] or impact energy [7]. Thus, the understanding of the driving factors of recrystallization and grain growth under cyclic HHF loads is essential for prediction of the lifetime of the PFCs [2,18].

In previous recrystallization studies, tungsten was mostly heat-treated under slow, quasi-uniform heating conditions. The recrystallization behaviour of tungsten in such stationary heating conditions is well documented in literature [9–14]. However, in HHF tests, simulating the expected heat loads during fusion reactor operation, cyclic HHF pulses with fast heating/cooling rates heat the water-cooled tungsten armor. The applied heat flux of 20 MW/m^2 generates a steep temperature gradient (20 MW/m^2 loading results in a gradient of about 200 K/mm) and high thermal stresses [14]. There are only a few studies dedicated to the recrystalization mechanism of tungsten under cyclic HHF [9,14–16]. For instance, a novel numerical approach was proposed by V. Shah *et al.* [15], which took into account the evolution of the recrystallized fraction during a cyclic HHF loading using a heat conduction model coupled with the recrystallization model by Johnson, Mehl, Avrami and Kolmogorov (JMAK model).

The distinct difference in heating conditions raises the question as to whether a furnace heat treatment (thermal radiation heating of the sample, quasi-isothermal temperature) properly simulates the cyclic HHF loading case in terms of recrystallization behaviour if the heat exposure time is kept comparable to each other. The present paper addresses this issue. We performed a comparative microstructural investigation study of two different groups of tungsten samples: one investigated after well-defined furnace heat-treatment conditions (1500 ℃, 2100 ℃) and the other one taken from monoblocks (at the positions of the same corresponding equilibrium temperatures) of a water-cooled PFC mock-up loaded with 500 cycles at 20 MW/m^2, 10 s heating, 80 s cooling down. The respective impacts of each heating condition on defect density, recrystallization, grain growth and hardness are investigated and compared for the equivalent cumulative heat exposure time based on extensive microscopic characterization (Scanning electron microscopy, SEM and Electron Backscatter Diffraction, EBSD) and quantitative image analysis. The behaviour of two different commercial tungsten grades (made by AT&M (PR China) respectively by ALMT (Japan)) are included in the study. This study is mainly focused on the effect of the steep temperature gradient and the thermal stress in the tungsten armor during the cyclic HHF loading of a water-cooled monoblock mock-up, which cannot be generated in the uniform furnace heating. Similarities and differences in the microstructural evolution between the two heating conditions are discussed.

2. Experimental methodologies

2.1. HHF exposure of water-cooled W mono-blocks

For this study we selected several DEMO-divertor mock-ups manufactured in the framework of the European DEMO development, work package 'Divertor' (WPDIV) [17]. Fig. 1 shows details of
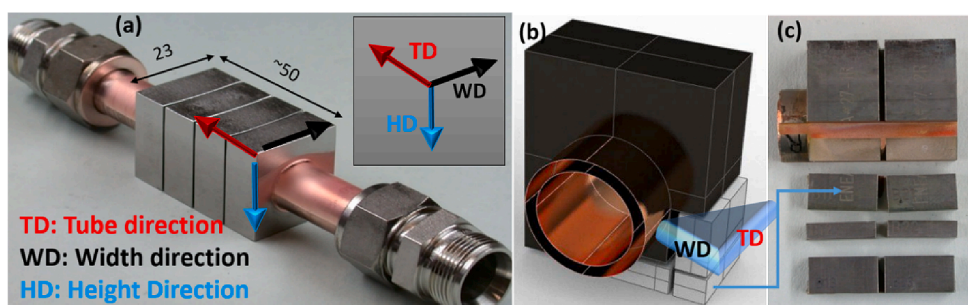
fabricated DEMO divertor mock-ups. Fig. 1b a schematic view of the sample arrangement, Fig. 1 c pictures of the cross-section after HHF loading and the samples provided for steady state heating (SSH) campaign along with introduction to different facets of the cuts, respectively. To avoid any inconsistencies due to material variations, samples for SSH campaign were cut from the cold part (below the cooling tube) of the same W mono-blocks that were previously used for HHF testing (see Fig. 1c). This ensures that the samples have not been subjected to thermally activated phenomena during the previous HHF tests. The processing directions were considered. Each cycle of HHF loading consists of four distinguished phases, heating, thermal equilibrium, cooling down, and a pause. The resulting equilibrium time is well proved by numerical and experimental studies as will be discussed in the coming sections [15,23].

The applied neutral hydrogen beam (150 mm full width at half maximum (FWHM)) ensures a simultaneous and homogeneous heating of all four blocks of the mockups. The outer mono-blocks are loaded with 95% of the central heat flux [20]. In the discussed testing campaign we used both, cold water cooling (15 ℃, 1 MPa) and hot water cooling (130 ℃, 4 MPa the cyclic HHF tests. The initial screening test were performed only with cold water-cooling. In case of mock-up "B", the initial screening was extended to 5 cycles of 30 MW/m^2 followed by 5 cycles at 32 MW/m^2 [20,21,24].

2.2. Steady-State heating (SSH) campaign

The purpose of the SSH experiments is to investigate the similarities and differences of the thermally activated phenomena in cyclic heat loaded compared to steadily annealed samples. The SSH campaigns were carried out on the surfaces parallel to the HHF-loaded parts in the W monoblocks (TD-WD facets as introduced in Fig. 1b). We calculated the annealing time (holding time at the target temperature) in SSH campaign to be the integral (sum) of the so-called equilibrium time per pulse for 500 HHF pulses (i.e., thermal cycles) and 1000 pulses (Fig. 2). We used a radiation furnace with helium (He) protective atmosphere (HORST) at IPP in Garching for this purpose. The specifications of HORST are reported in detail elsewhere [25].

In the steady state heating (SSH), the cyclic nature of the fast heating and cooling of samples in the repeated HHF pulses is absent. In our study, only the cumulative effects of equilibrium heating of all pulses were taken in account as to be an equivalent time for the isochronous annealing. Hence, the individual temperature lines of HHF are taken into consideration for the corresponding SSH campaign as annealing temperature. The dynamic evolution of the microstructure during each cycle of HHF is not in the scope of our study.

The 20 MW/m^2 HHF testing results in a wide range of temperature fields throughout the HHF-loaded part of the mono-blocks (from 200 to 2100 ℃). The temperature dependence of material properties such as the thermal conductivity (κ), the product of mass density and the specific heat ($c\rho$) for the W, Cu and heat sink layer of CuCrZr alloy are considered

Fig. 1. (a) DEMO Tungsten mock-up, the water connecter on both ends are visible. And (b) A three dimension sketch of the water-cooled tungsten monoblock and the cross-section after loading in the HHF test facility GLADIS. The mock-ups were manufactured by ENEA [17]. (c) The cuts for SSH campaign with corresponding laser etched labels. All dimensions are given in millimetres. The monoblocks have an armour thickness of 8 mm. The cuts for SSH test are provided from the down half of the mock-up (b and c), which were not, exposed directly to HHF neutral hydrogen beam and WD-TD surfaces (parallel to the HHF has been polished for further observation.
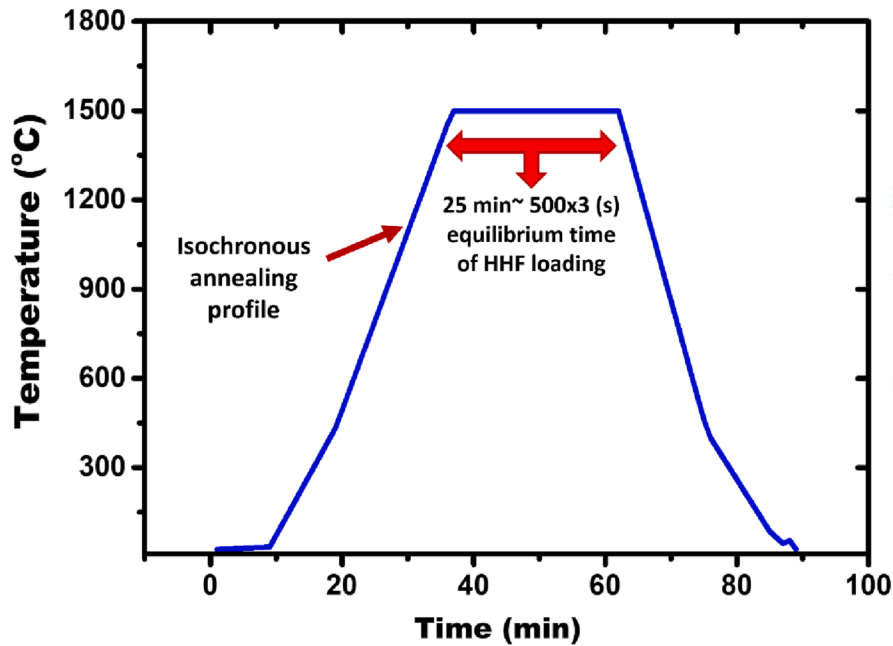
Fig. 2. Annealing and cooling cycle (Temperature-time) of a W sample in the SSH campaign.

in the numerical modelling of the temperature fields throughout the monoblocks [26]. Referring to the most recent published results [15], for the same monoblocks and similar test conditions, we have taken the calculated activation energies of moderately deformed tungsten as an input for this study. Fig. 2 depicts a typical annealing and cooling cycle of a DEMO-like divertor mock-up in our SSH campaign and compares that with a single pulse of HHF at GLADIS. The number of pulses were 500 at the fixed power density.

2.3. Microstructural analysis

To quantify the microstructure dependent mechanical behaviour, we carried out the microstructural examination via EBSD technique. The samples from the monoblock were obtained through electrical discharge machining (EDM). To avoid all the material affected by the cutting procedure and induced damage, we removed the topmost $\sim 200\ \mu m$ of the cut surfaces during the surface preparation. Specimens corresponding to the WD-TD (x-z) plane of the monoblock from the initial (Fig. 1b and c) and recrystallized state were prepared by mechanical grinding using SiC paper (up to P4000), followed by electro polishing with 1.5 wt% NaOH (sodium hydroxide) solution at 15 V for approximately 120 s.

A HELIOS NanoLab 600 scanning electron microscope equipped with a Ga$^+$ Focused Ion Beam (FIB) and Oxford Instruments EBSD system was used to acquire microstructure images and EBSD maps. An acceleration voltage of 25 kV along with a working distance of 10 mm was used for all mappings, while the lateral step size was varied depending on the microstructural state. The FIB technique allowed creating markers on the samples to keep track of a specific region on the sample after multiple sequential heat treatments in SSH campaign. In case of the initial state, an area of $1.25 \times 1\ mm^2$ was mapped with a step size of 0.5 μm, whereas for the recrystallized state, an area of $1.25 \times 1\ mm^2$ was mapped with a step size of 1 μm. The EBSD map data was subjected to two clean-up procedures, i.e., grain dilation clean up and neighbour confidence index (CI) correlation. Additionally, the indexed points with a CI less than 0.1 were ignored for post-processing, which was performed using the Aztec Software from Oxford Instruments and exported into Oxford-HKL Channel 5 [27].

We characterized the grain boundaries in the EBSD maps based on the misorientation between adjacent data points. The standard definition of the grain boundaries following the work of Humphreys [28], was adopted in the present work, i.e., boundaries with a misorientation angle between 2° −10° are classified as low-angle (LAGBs), whereas boundaries with misorientation angle > 10° are termed as high-angle (HAGBs) [10,29].

3. Results and discussion

3.1. Recrystallization in different temperature fields of HHF tested mock-ups

Recrystallization is a thermally activated process, the extent of which depends on the annealing temperature and the time of exposure to that temperature for a specific material. Accordingly, throughout the HHF-loaded part of the monoblocks, the resulting microstructure varies with respect to the equilibrium temperature reached in each region of the monoblock. For defining the temperatures to be used in SSH experiments, we refer to the numerical FEM simulations of the temperature fields throughout the DEMO-like monoblocks during HHF loading [15,30]. As a reference model for the study, the DEMO-like baseline design was investigated for lifetime assessment [26]. In the current discussions, we focused on the temperature fields with respect to the depth from the HHF-loaded surface.

For isothermal conditions, the kinetics of recrystallization can be described by the JMAK model [4] given as: [6]

$$X = 1 - \exp(C(t/t_{50})^n) \qquad (1)$$

In equation (1), X: recrystallized fraction, C: a constant (equal to −0.7, considering 50% recrystallization, i.e. ln (0.5)), n: representing the Avrami exponent, and t_{50}, representing the time required to achieve 50% recrystallization. Furthermore, considering the temperature dependence, the time to half recrystallization t_{50} can be expressed as:[4]

$$t_{50} = t_{50}^0 \exp\left(\frac{E_{act}}{RT}\right) \qquad (2)$$

t_{50}^0: Pre-exponential factor, E_{act}: activation energy for recrystallization, R: real gas constant and T: annealing temperature.

The activation energy generally depends on the history of deformation. This input for the above calculations is based on the isochronous annealing experiments [10]. A constant Avrami exponent of n = 2 was

used for all our simulations. According to the numerical studies, the influence of the exact value of the Avrami exponent on the recrystallization behaviour of the mono-block was shown to be insignificant in the computation modelling [29]. An activation energy in the range 322 to 350 kJ/mol corresponding to the recrystallization driven by grain boundary diffusion has been taken from recrystallization in different cyclic HHF-loaded mono-blocks using an inverse methodology experiments and numerical simulation [15,29,31,32]. The results, as expected, demonstrate that the recrystallization volume through the depths of monoblock with respect to the number of cycles is highly sensitive to the input activation energy for the initial tungsten material [15].

Fig. 3a illustrates the numerically simulated temperature fields in the mono-block at the end of a 10 s pulse for 20 MW/m^2 heat density load at the edge of the monoblock [23]. This finite element modelling (FEM) result is calculated for a high heat flux at an assumed coolant temperature of 150 °C. The evolution of the recrystallized fraction of mono-block during the high heat flux campaign between the cooling channel and the top surface is calculated in another study [15]. Fig. 3b and c show the calculated (time vs. temperature) and real time pyrometer (2 different types in caption of image 3) data for surface temperature versus time of a single pulse for the 20 MW/m^2 heat flux test under hot water-cooling conditions, respectively. Both results are in reasonable agreement for the equilibrium time and surface temperature of a single pulse. According to these insightful results of experiment and numerical calculations, the thermal equilibrium time of a 10-second 20 MW/m^2 heat pulse is ∼ 3 s. Hence for the SSH campaign, we accordingly defined the steady-state annealing time to be 1500 s, which corresponds to 500 HHF pulses. In addition, we performed SSH experiments with twice this flat-top duration, i.e., of 3000 s. These were meant to determine whether the exact duration of the SSH annealing would have a measurable influence on the resulting grain size, since our definition of the equilibrium time during HHF testing is to some degree arbitrary.

The FEM calculations also clearly showed that the lower part of the monoblock from which the samples for the SSH campaign were cut, have not been exposed to temperatures above approximately 300 °C during HHF testing (Fig. 3a, half down part of the monoblock). Hence, the annealing for the bottom part did not exceed the temperature that was reached during joining of the coolant pipe to the monoblock in the manufacturing process of the mock-ups [33].

3.2. Microstructure analysis before and after HHF

Fig. 4a and b show the optical microscope images of the cross-section of the two different DEMO-like divertor monoblocks from the cooling channel to the topmost surface after 500 cycles of 20 MW/m^2. We collected the corresponding EBSD maps from the topmost surface and merged in horizontal direction in the corresponding optical images. The formation of huge grains on the topmost surface (T ∼ 2100 °C) along with the visible transition line between recrystallized and non-recrystallized region at T ∼ 1200°C, are highlighted for both mono-blocks (taken from mock-ups "B" and "C"). The W producer and the HHF campaign for these two mock-ups, "B" and "C", are different; as a result, we observe quite different patterns of grain evolution at the topmost surface at 2100 °C. As seen in Fig. 4a and b, abnormal grain growth is more encouraged in case of mock-up "B", which was initially exposed to a number of cycles with very high heat fluxes (32 MW/m^2) and cold water-cooled during all HHF tests (Table 1).

We performed corresponding scanning electron microscope (SEM) imaging and EBSD mapping of the microstructure in the longitudinal direction of the cross-section of the HHF monoblocks. The results are demonstrated in the supplementary materials S1. The numerical study done by V. Shah et al. [15], proved the recrystallization volume that occurs in the first single pulse of 20 MW/m^2 HHF with hot water cooling extends to 3.5 mm down from the surface of similar DEMO divertor monoblocks. For 1000 cycles of HHF, the numerical calculation outcome showed that the full recrystallization volume could be expected to extend to 5.2 mm distance from the top surface. The temperature of 2100 °C is the maximum surface temperature of the monoblocks during the equilibrium phase of 20 MW/m^2 pulses, as shown by measurements and calculations (Fig. 4)[28].

Having observed all the details in Fig. 4, there is a negligible difference in the degree of the recrystallized volume and microstructure of the recrystallized grains in the temperature fields between ∼ 1300 and 1900°C. In other words, in this region of the sample, grain growth is effectively limited to the observed degree by the manufacturing procedure of the tungsten. The history of the tungsten manufacturing has not been fully disclosed by the tungsten manufacturers. It is well documented that the whole manufacturing process of W (rolling, thickness reduction, etc.), influences the activation energies of recrystallization related to grain boundary diffusion [14]. Nevertheless, it is a general desired property of the fusion grade tungsten to inhibit excessive grain growth while exposed to cyclic high heat fluxes. Furnace annealing also confirms the resistance of the investigated W grades (A.L.M.T and AT&M) against excessive grain growth, as will be discussed in Section 3.3.

Fig. 5a and b show the microstructure and high angle grain boundary (HAGB) map observed in the as-received tungsten from the producer AT&M after mock-up fabrication and before any HHF loading (Mock-up "A"). Fig. 5a displays an inverse pole figure (IPF) map obtained from EBSD. Due to the rolling process conducted in the tungsten
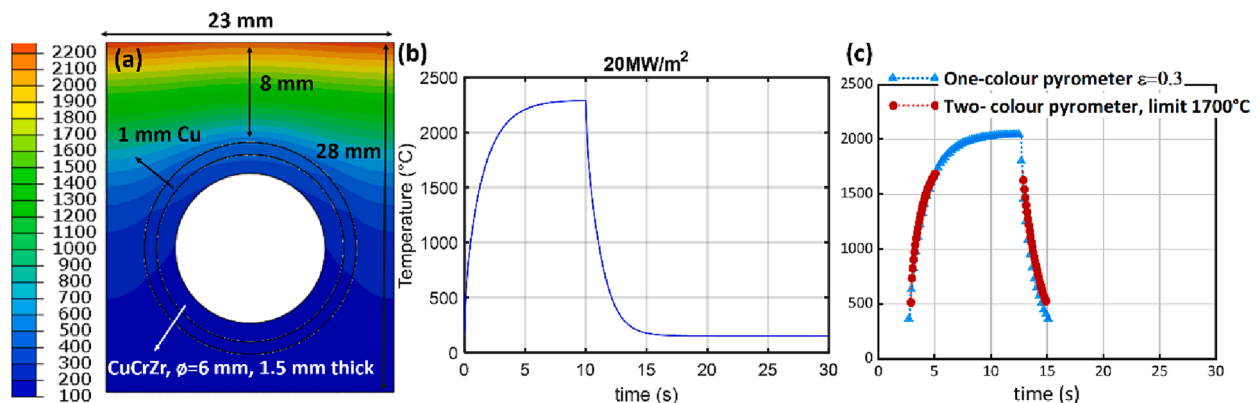

Fig. 3. (a) Temperature field and surface temperature diagram of a mono-block at the end of 10 s exposure of 20 MW/m^2 surface heat load [23]. The dimensions of the elements of the mock-up are shown in the image (a). The temperature trace of graph (b) belongs to the outer corners of the monoblock. The FEM result is computed for a high heat flux load at a coolant temperature of 150 °C and (c) Surface temperature evolution of the centre of a W monoblock during a 10 s, 20 MW/m^2 cycle in GLADIS. The temperature is measured by two different pyrometers: one-color and two-colors. The temperature is slightly lower as in graph (b) since the central temperature is lower as the shown edge temperature. Note graph b and c share the same Temperature (y) axis.
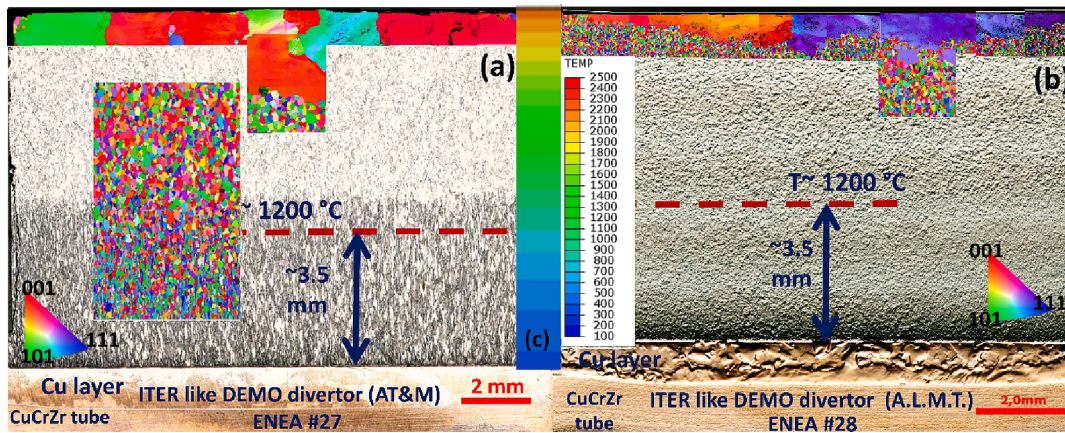
Fig. 4. Optical microscope images and corresponding EBSD derived inverse pole figure (IPF) of the axial cuts of W monoblocks of two different DEMO-like divertor mock-ups "B" and "C". The CuCrZr cooling channel and the Cu interlayer are shown in the lower part of the images. (a) Mock-up B, manufactured of AT&M tungsten, and (b) mock-up C, manufactured of A.L.M.T tungsten. The recrystallization started about 3.5 mm about the W/Cu interface. (c) The simulated temperature field across the monoblock in the HHF test at 20 MW/m² to better indicate the transition of non-recrystallized to fully crystallized grain region.

Table 1
List of tested mock-ups, HHF tests parameters and steady state annealing conditions.

Mock-ups	A: ENEA#24	B: ENEA#27	C: ENEA#28
Spécifications			
Tungsten Block: Types and producers	Block type **4–71 Produced by AT&M PR China	Block type *3–09,10,11,12 Produced by AT&M PR China	Block type** 4 Al-36 and AL-37 Produced by A. L.M.T Japan
Applied heat flux (MW/m²)	screening up to 25	screening up to 32	screening up to 25
Number of cycles	500 × 20 MW/m²	100 × 21 MW/m²	500 × 20 MW/m²
Cooling condition	hot water 130 °C, 16 m/s, 4 MPa	cold water 20 °C, 12 m/s,1 MPa	hot water 130 °C, 16 m/s, 4 MPa
Pulse duration (heating/ cooling)	10 s/ 80 s	10 s/ 80 s	10 s/ 80 s
Average surface temperature in steady-state	2050 ± 100 °C	2100 ± 100 °C	2050 ± 100 °C
SSH test conditions (annealing)	@1500 and 2100 °C - for 0.5 and 1 h	@1500 and 2100 °C - for 0.5 h	@1500 and 2100 °C - for 0.5 h

*,** type 3 and 4 are different in the thickness of the Cu interlayer, (0.3 mm for type 3 and 1 mm for type 4).

manufacturing procedure, grain sub-division and ultimately the formation of smaller grains having a misorientation of less than 10° are encouraged. Also, a large fraction of the grains in the width direction (WD) IPF map exhibit a preferred crystal orientation of ⟨1 1 0⟩||WD. This is reflected by the green colour code in the IPF map.

Fig. 5c and d correspond to the region were the flat-top temperature is about ~ 1500 °C during HHF loading. The width direction (WD) IPF map for the recrystallized microstructure is shown in Fig. 5c and a significant difference in the geometry of the recrystallized grains can be observed as compared to the initial grains in Fig. 5a. The recrystallized grains tend to exhibit a more equiaxed morphology, which is clear from the high angle grain boundary map shown in Fig. 5d. The grains in the recrystallized state tend to be relatively coarse with only a small fraction of fine grains, which further indicates the occurrence of substantial grain growth. Additionally, the fraction of grains shaded in green is considerable, thereby indicating a ⟨1 1 0⟩||WD type preferred crystal

orientation. The grain growth is dominated by high surface energy anisotropy, which prevents most boundaries from moving [10,11]. Those grains whose boundaries could still move eventually dominate the microstructure at the end of cumulative HHF cycles. It is noteworthy that even though the starting microstructure is a rolled texture with elongated grains, many of the triple junctions that develop, even in the apparently stable finer-grained material, do NOT evolve to 120°, which would be the equilibrium angle if there was no surface energy anisotropy [9].

The thickness reduction caused by rolling of tungsten, have introduced a certain amount of strain and high-density dislocation regions in the microstructure [10–12] and consequently affected the activation energy for recrystallization during HHF loading as discussed in previous section (3.1). The significant reduction in the density of defects inside the grains after 500 cycles of HHF compared to the initial, highly-deformed state, which typically occurs during recrystallization, can be translated to more activation energy required for further evolutions from this current status [11].

Having an observation on two resulting microstructures of pre and post-HHF at 1500 °C, now we are ready to extend our comparison to post-HHF versus post-SSH campaigns.

3.3. SSH vs. HHF for 1500°C and 2100 °C

Figs. 6 and 8 show an inverse pole figure (IPF-Z) and (IPF-Y) maps and grain boundary maps driven from EBSD of the post-annealing examination (SSH) vs. post-HHF loading AT&M tungsten (Mock-up "B" and "A" respectively). Whereas Fig. 7, represents the corresponding quantitative data obtained from the collected EBSD maps on the grain diameter distribution.

In Fig. 6, a large fraction of the grains in the height direction (HD) IPF map are coloured red, thereby revealing a preferred crystal orientation of ⟨0 0 1⟩||HD. The resulting maps indicate some points as following:

1. After 1500 °C campaigns, grains in resulting microstructures tend to become more symmetric compared to the initial microstructure, although some traces of the initially prominent grain elongation remain. Grain boundary misorientations and orientation texture of the grains are very similar in both HHF and SSH (note that scales are bigger in SSH resulting maps). The average grain sizes were collected and derived from the EBSD maps by using the Oxford HKL Channel 5 software and plotted in Fig. 7. We concluded that the
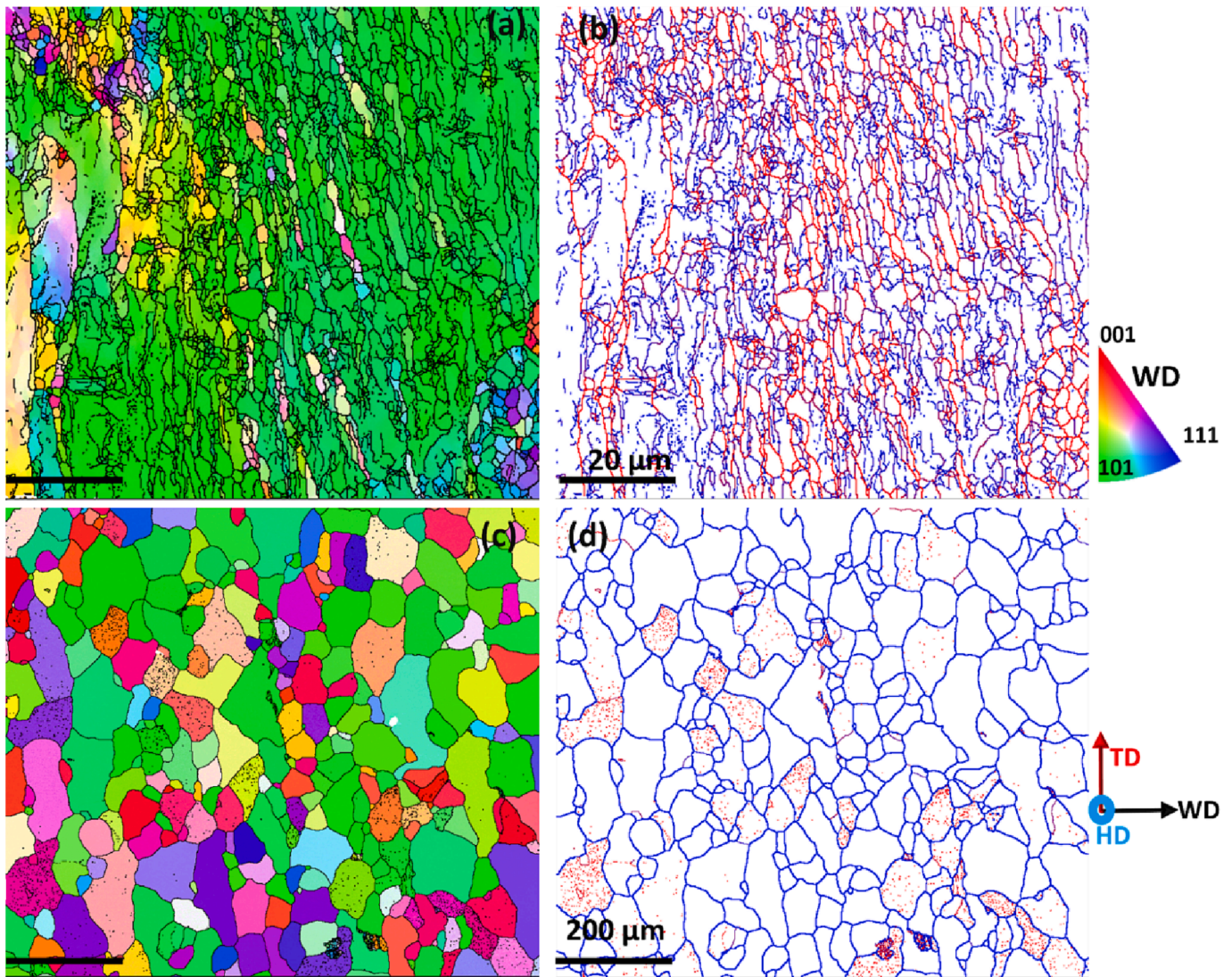
Fig. 5. Inverse pole figure (IPF-Y) EBSD maps corresponding to the texture and grain structure of (a and b) the as-received tungsten from Mock-up "A" (AT&M tungsten) after fabrication and before HHF loading, (c and d) the same monoblock after exposure to 500 cycles of 20 MW/m². Figures b and c correspond to a temperature of 1500 ℃. The blue and red lines in the EBSD maps indicate the high-angle and low-angle grain boundaries respectively. The grain boundaries with angles>2° and smaller than 10° are considered as low-angle grain boundaries. (For interpretation of the references to color in this figure legend, the reader is referred to the web version of this article.)

recrystallization is fully completed after both SSH and HHF campaigns at 1500 ℃.

2. Fig. 7 plots the calculated grain sizes with respect to their cumulative probability of distribution in the measured area for the SSH and HHF campaigns. It is noteworthy that the grains have grown to very similar sizes at 1500 ℃, irrespective of the heating method. In addition, the grain diameter distribution is quite narrow. As observed in Fig. 7, for the temperature of 2100℃, after 100 cycles of HHF loading, the grain diameters are not significantly larger than at 1500 ℃ if one excludes the abnormally large grains immediately below the sample surface. This trend can be clearly seen in Fig. 6 d and h. This is not a typical behaviour of tungsten and in literature it is well documented that tungsten grains may grow to very large sizes after a certain time and temperature (>1900 ℃) depending on the annealing cycle [9,10,25,34]. The fact that the majority of grains in HHF tested samples and SSH ones at 2100 ℃ are hindered from overly growing, is a key property of W developed for fusion application[17]. The grain diameter distribution of the resulting microstructure after SSH campaign at 2100 ℃ has a large overlap with the data collected from the 1500 ℃ SSH campaign with a small

extension toward grain sizes > 100 μm and slightly larger width. For plotting the data in Fig. 7, we have disregarded the abnormally enlarged grains of the topmost surface of HHF loaded sample.

3. After 2100-℃ campaign, the grains at the topmost surface of HHF tested samples are overly grown and highly deformed in both mock-ups (Fig. 6g and 8 g). This did not occur in SSH experiments; even if the annealing time was extended from, 1500 to 3000 s (see also below). This abnormal grain growth near the surface of the HHF samples is a distinct consequence of the cyclic HHF heating.

4. Tracking the same area for imaging and EBSD mapping after 1500 and 2100 ℃ campaigns in Fig. 6, we observe grains that are mostly preserved but developed more curved facets. Black crosses in Fig. 6b and are indicating these grains. This rare observation based on tracking the single grains after two consecutive SSH campaign shows that the recrystallized grain structure created at 1500 °C is remarkably stable against further grain growth up to at least 2100 °C. The few small grains that are consumed during the growth of adjacent grains are also tracked in both temperatures and indicated by black dotted circles in Fig. 6b and d. This result may verify the numerically calculated recrystallized volume vs. number of HHF cycles by V.
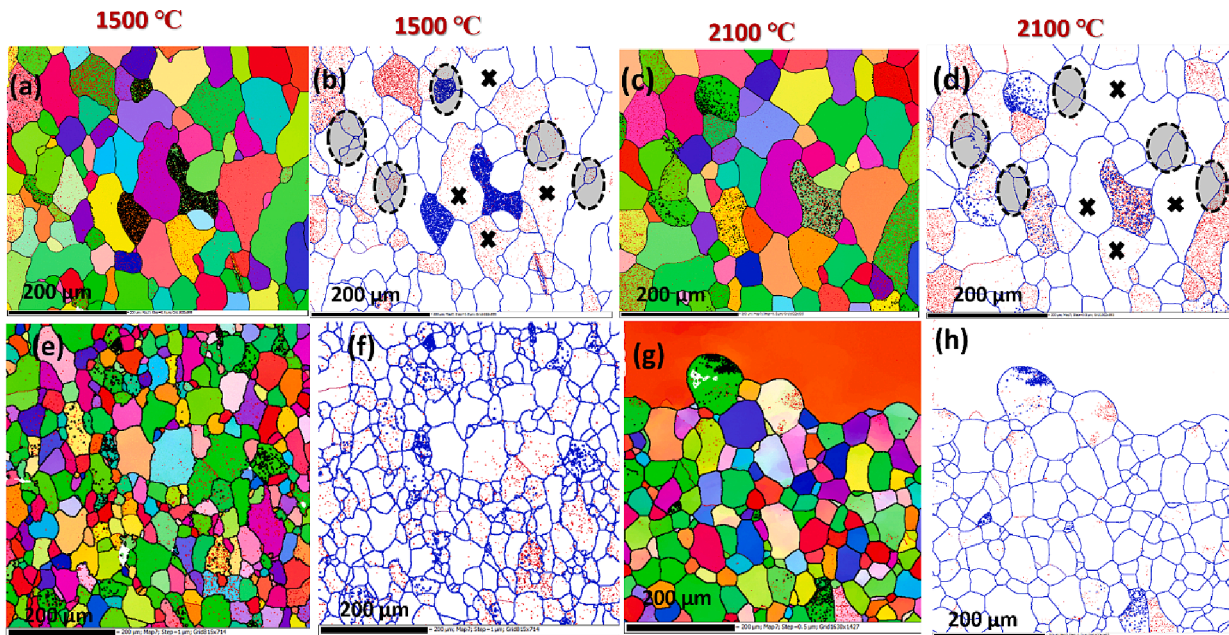
Fig. 6. Inverse pole figure EBSD maps (IPF-Z) for post-annealing examination (a-d-upper row images) vs. post HHF(e-h lower row of images) for the mock-up "B" (AT&M tungsten). A screening up to 32 MW/m² and subsequent cycling of 100 cycles at 21 MW/m² were performed according to Table 1. The black crosses indicate the grains, which are almost intact after 1500 °C and proceeding 2100 °C SSH annealing. The black dotted circles indicate the grains that have been consumed by adjacent grains or grown comparing the 1500 and 2100 °C-annealed microstructure. The blue and red lines in the EBSD maps indicate the "high"-angle and "low"-angle grain boundaries respectively. (For interpretation of the references to color in this figure legend, the reader is referred to the web version of this article.)
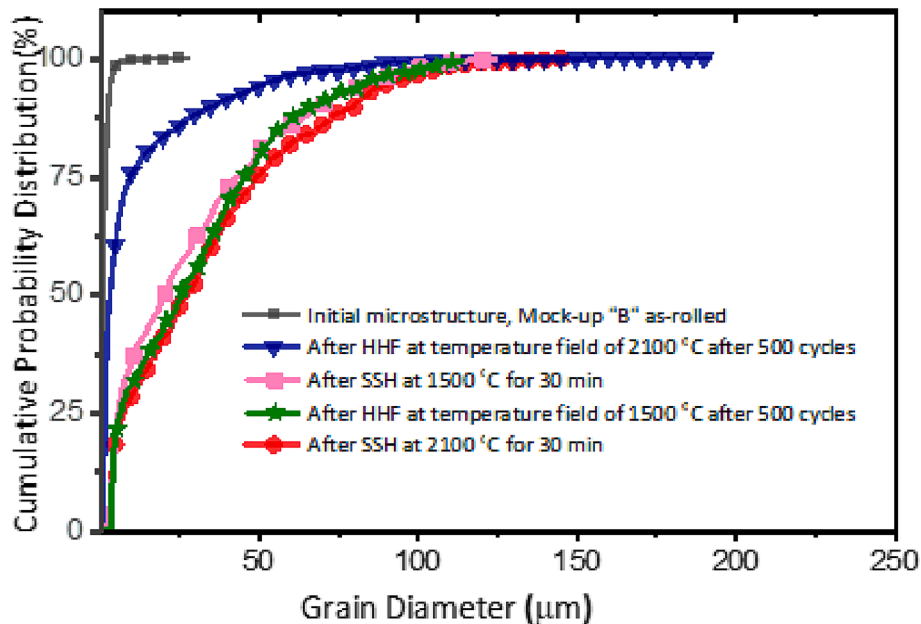

Fig. 7. Cumulative grain diameter distribution in the resulting microstructures after HHF and SSH campaigns for mock-up "B".

Shah et al. [15]. The microstructural evolution in the bulk of HHF tested samples appears to be slowing down for the temperature fields of 1300 to 1900 °C and further cycles will not cause a remarkable change in the microstructure. This result in a similar way concerns the higher activation energy barrier created in the microstructure after one-step SSH campaign.

5. The spheroidized grains are more prominent at 2100°C in both resulting microstructures of SSH and HHF (Fig. 6g and 8 g). This is due to the surface energy and inter-grain tension forces. In the furnace annealing, rather than a huge heat flux of the unidirectional beam, a homogeneous radiative heating and sufficient time encourages more curvature in grain recrystallization [31].

6. Detailed EBSD analysis of mock-up "A" in Fig. 8 reproduced the majority of the results obtained for mock-up "B" analysis. Except for the topmost surface, there are no remarkable differences in recrystallization results for different cooling conditions during HHF experiments (hot and cold water-cooling) as well as for overloading, screening and normal cycling.

All the three mock-ups of "A and C at their topmost surface after 500 cycles of HHF and B after 100 cycles of HHF are examined. The loading
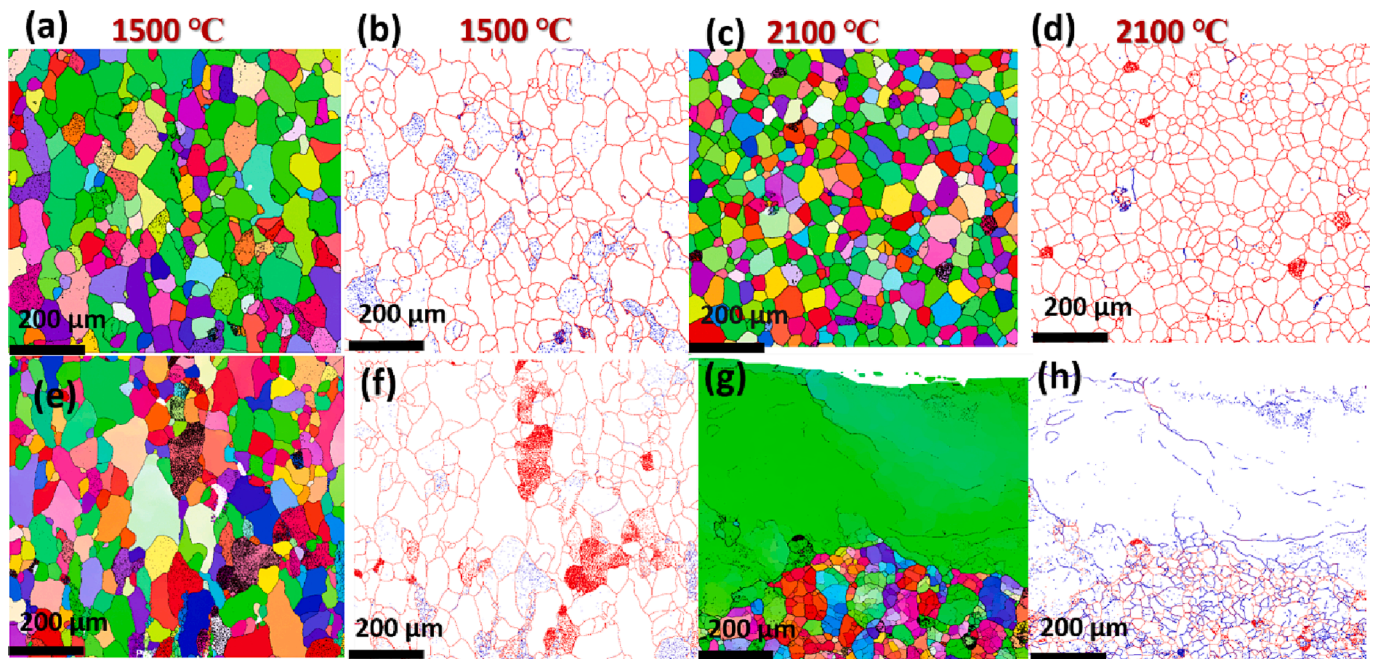
Fig. 8. Inverse pole figure driven EBSD maps (IPF-Y) for post annealing examination, SSH (a-d, upper row of images) vs. post HHF (e-h, lower row of images) for the mock-up "A", AT&M tungsten producer. The HHF loading consists of cycling for 500 cycles at 20 MW/m^2 with hot water cooling (Table 1). The blue and red lines in the EBSD maps indicate the low-angle and high-angle grain boundaries respectively. (For interpretation of the references to color in this figure legend, the reader is referred to the web version of this article.)

with different cooling water temperatures (20 °C and 150 °C) as well as different heat flux densities are explained in Table 1. Both tested tungsten grades (A.L.M.T and AT&M) behave relatively similar at the topmost surface after loading ≥ 20 MW/m^2. Detailed SEM images, EBSD and colour code grain boundary maps are provided in supplementary materials in Figure S2. The overly grown grains on the topmost surface are the common attribute of all different mock-ups regardless of the heat flux density and maximum temperature of the topmost zone in these three samples (Table 1). It is noteworthy that similar HHF tests, performed in electron beam devices have observed the similar phenomena [15,30,31]. Near the topmost surface, a considerable number of LAGBs

can be found inside the excessively grown grains.

In order to investigate the defect structure of the deformed, excessively grown grains, we used high-resolution backscattered electron images. In many locations of the topmost surface of the mono-block "A" after HHF, the grain orientation was suitable for electron channelling contrast imaging (ECCI) [35]. (See also Fig. 8 g and h). Fig. 9 shows an ECCI image of the mono-block "A" after 500 cycles of 20 MW/m^2 HHF with hot water-cooling. The magnified images in Fig. 9d and g reveal regions with a high density of dislocations, which are indicated by red arrows. The grayscale gradients inside the large grains are another feature of the deformation in the large grains. This high dislocation
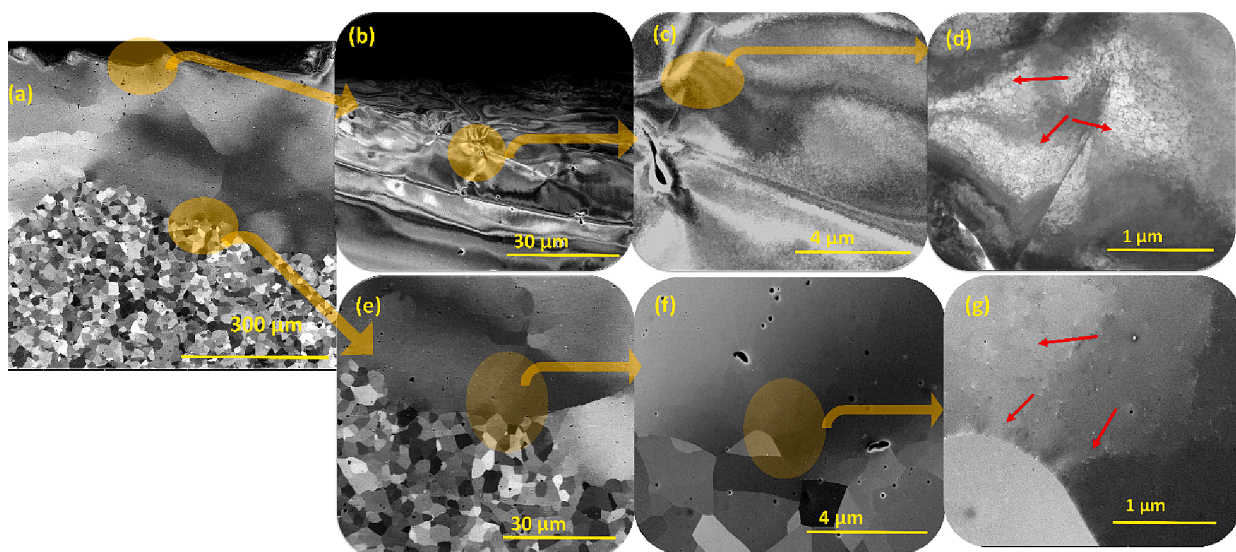

Fig. 9. Electron channelling contrast imaging (ECCI) corresponding to the grain boundary and EBSD maps of the top most surface of the mono-block "A" after 500 cycles at 20 MW/m^2. The focus of high magnification images are the grains at the topmost surface i.e., in the temperature field of 1900–2100 °C. Red arrows indicate the dense dislocation clusters/lines and the grayscale gradients inside the large grains is another feature of the deformation in the large grains. (For interpretation of the references to color in this figure legend, the reader is referred to the web version of this article.)

density affects the microhardness values of this region of the mono-blocks (flat-top temperature 1900–2100 ℃) after the HHF campaign as will be discussed in the following.

3.4. Microhardness values of tungsten mono-blocks after SSH and HHF

In order to assess the mechanical properties of the samples after HHF or SSH heating correlated with their recrystallization behaviour, we also performed Vickers microhardness tests on the surfaces described in the previous sections. As shown in Fig. 10a, the hardness values for the samples from the HHF mock-ups "A" and "C" are reduced by about 15 % compared to the initial value (measured near the cooling channel) after recrystallization starts, i.e., in the region where the temperature reached 1300 ℃ and above. In Fig. 10(a), the result seems to be in agreement with our recrystallization evolution tracking with EBSD mapping in the cross-section of the mock-ups in Fig. 4. In addition, here, the recrystallized region showed a rather clear boundary where the temperature calculated by FEM was about 1300 ℃. For both mock-ups, the hardness values vary only slightly up to the loaded surface. For mock-up "C", there might even be a marginal increase of hardness close to this surface.

Fig. 10b highlights the remarkable difference of hardness values at 2100 ℃ between the two campaigns of SSH and HHF for A.L.M.T and AT&M tungsten materials. The considerable softening that happened after furnace annealing after 2100 °C is in agreement with hardness values that are reported in literature about the behaviour of standard W grades [36](i.e., W grades not specifically designed for resilience against recrystallization, in contrast to mock-ups "A" and "C") after high temperature steady state annealing [15,30,31]. There, an exponential decrease of hardness withe time and temperature of the annealing is well-proven by other researchers [25]. After SSH annealing at 1500 °C, the material, by design, retains a considerable amount of hardness. However, the HHF-heated materials show a higher hardness in the equivalent temperature region. Furthermore, the high hardness on the topmost surfaces of HHF loaded mock-ups, which is comparable to the hardness of the initial material, is somewhat unexpected.

We assume this hardening at the topmost surfaces after HHF campaign is due to the high degree of deformation in the region near the HHF-loaded surface. These grains in this region contain a high dislocation density as well as many LAGBs, similar to the original rolled material. To some extent, this is also the case for grains further from the HHF surfaces: some of the grains below the huge top grain contain dislocations and LAGBs (Fig. 9). The dislocations would probably be integrated into the huge grain in the course of time and at temperature of 2100 °C. This interpretation of our investigations could explain the slightly higher hardness of the HHF samples compared to SSH also there.

4. Conclusions

We investigated the change of the grain structure and hardness induced by recrystallization and grain growth by the steady state heating (SSH) and cyclic high heat flux loading of DEMO divertor W mock-ups. The following conclusions can be drawn from the results:

1. For both investigated W grades (suppliers: AT&M (PR China) and A.L.M.T (Japan)) a temperature of 1500 °C resulted in recrystallization and yielded comparable microstructures and Vickers hardness values, regardless of the cyclic or steady-state heating. This is consistent with theoretical calculations (see [15]). Since the total number of test cycles respectively annealing time was relatively short in our study, recrystallization throughout a large part of W monoblocks can be expected during regular operation in a nuclear fusion reactor.
2. Vickers hardness measuring after 500 cycles of 20 MW/m^2 and hot water cooling showed only a minimal reduction in hardness throughout the W monoblocks, despite the samples reaching temperatures of about 2100 °C for a cumulative time of approximately 1500 s. On the other hand, SSH at 2100 °C resulted in more than a factor 4 of hardness reduction compared to the initial material.
3. Post-SSH analysis proved that steady state heating of the investigated W grades leads to a homogenous recrystallized microstructure with a relatively narrow grain size distribution at temperatures of 1500 and 2100 °C. The grains became only marginally larger at 2100 °C compared to 1500 °C, also in direct comparison of the same grains on a sample annealed first at 1500 °C and subsequently at 2100 °C (see Fig. 6 a-d).
4. During HHF loading, very large grains (~mm) were generated at the surface of the monoblocks. These grains showed strong deformation as well as a high density of dislocations and low-angle grain boundaries. Such excessive grain growth did not occur in SSH at the same temperature of 2100 °C and therefore is a consequence of cyclic HHF loading. The high degree of deformation in these grains is presumably responsible to the high hardness observed in Vickers testing of these samples, in contrast to SSH at the same temperature.

CRediT authorship contribution statement

Narguess Nemati: Methodology, Investigation, Data curation, Formal analysis, Visualization, Conceptualization, Writing – original draft, Writing – review & editing. **A. Manhard:** Conceptualization, Methodology, Methodology, Validation, Supervision, Writing – review & editing. **H. Greuner:** Conceptualization, Validation, Resources, Project administration, Writing – review & editing. **K. Hunger:** Software,
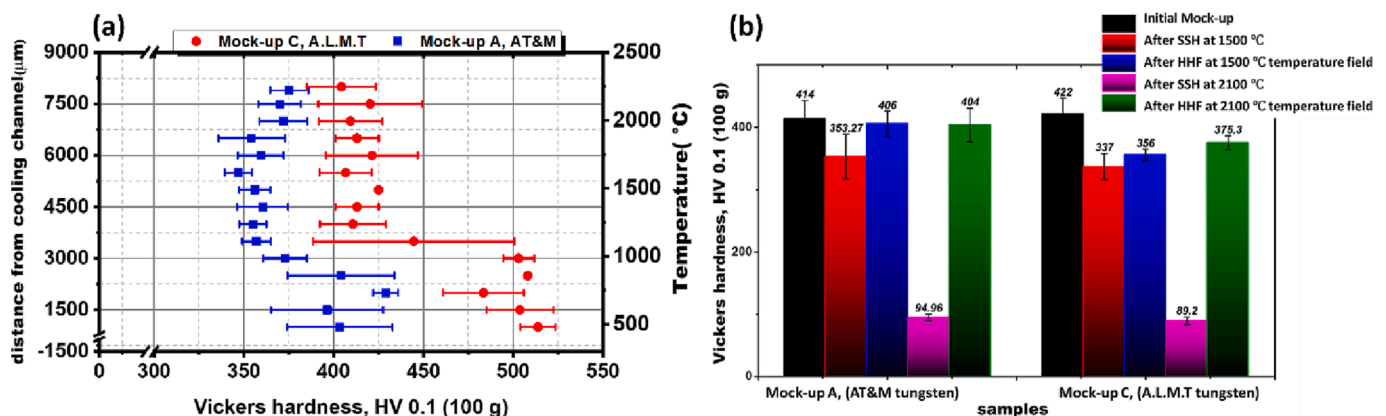
Fig. 10. (a) Vickers microhardness values with respect to the temperature field (position) of the Mock-ups "A and C" after HHF campaign. Note that the zero to 300 value of the hardness axis has been suppressed for better visualization. (b) Comparison of the resulting average Vickers microhardness values after different campaigns (SSH and HHF) with respect to the mock-ups and tungsten producers.

Methodology. **B. Böswirth:** Data curation, Methodology, Resources. **E. Visca:** Validation, Resources. **J.H. You:** Funding acquisition, Project administration, Supervision.

Declaration of Competing Interest

Data availability

Data will be made available on request.

Acknowledgment

Appendix A. Supplementary data

Supplementary data to this article can be found online at https://doi.org/10.1016/j.nme.2023.101465.

References

[1] G. De Temmerman, T. Hirai, R.A. Pitts, The influence of plasma-surface interaction on the performance of tungsten at the ITER divertor vertical targets, Plasma Phys. Control. Fusion. 60 (2018), https://doi.org/10.1088/1361-6587/aaaf62.

[2] C. Yin, D. Terentyev, T. Pardoen, R. Petrov, Z. Tong, Ductile to brittle transition in ITER specification tungsten assessed by combined fracture toughness and bending tests analysis, Mater. Sci. Eng. A 750 (2019) 20–30, https://doi.org/10.1016/j.msea.2019.02.028.

[3] S. Bonk, J. Hoffmann, A. Hoffmann, J. Reiser, Cold rolled tungsten (W) plates and foils: Evolution of the tensile properties and their indication towards deformation mechanisms, Int. J. Refract. Met. Hard Mater. 70 (2018) 124–133, https://doi.org/10.1016/j.ijrmhm.2017.09.007.

[4] C. Ren, Z.Z. Fang, L. Xu, J.P. Ligda, J.D. Paramore, B.G. Butler, An investigation of the microstructure and ductility of annealed cold-rolled tungsten, Acta Mater. 162 (2019) 202–213, https://doi.org/10.1016/j.actamat.2018.10.002.

[5] H. Bolt, V. Barabash, G. Federici, J. Linke, A. Loarte, J. Roth, K. Sato, Plasma facing and high heat flux materials - Needs for ITER and beyond, J. Nucl. Mater. 307–311 (2002) 43–52, https://doi.org/10.1016/S0022-3115(02)01175-3.

[6] V. Philipps, Tungsten as material for plasma-facing components in fusion devices, J. Nucl. Mater. 415 (2011) S2, https://doi.org/10.1016/j.jnucmat.2011.01.110.

[7] J. Reiser, M. Rieth, B. Dafferner, A. Hoffmann, X. Yi, D.E.J. Armstrong, Tungsten foil laminate for structural divertor applications - Analyses and characterisation of tungsten foil, J. Nucl. Mater. 424 (2012) 197–203, https://doi.org/10.1016/j.jnucmat.2012.02.030.

[9] K. Tsuchida, T. Miyazawa, A. Hasegawa, S. Nogami, M. Fukuda, Recrystallization behavior of hot-rolled pure tungsten and its alloy plates during high-temperature annealing, Nucl. Mater. Energy. 15 (2018) 158–163, https://doi.org/10.1016/j.nme.2018.04.004.

[10] P. Lied, C. Bonnekoh, W. Pantleon, M. Stricker, A. Hoffmann, J. Reiser, Comparison of K-doped and pure cold-rolled tungsten sheets: As-rolled condition and recrystallization behaviour after isochronal annealing at different temperatures, Int. J. Refract. Met. Hard Mater. 85 (2019), 105047, https://doi.org/10.1016/j.ijrmhm.2019.105047.

[11] U.M. Ciucani, A. Thum, C. Devos, W. Pantleon, Recovery and recrystallization kinetics of differently rolled, thin tungsten plates in the temperature range from 1325 °C to 1400 °C, Nucl. Mater. Energy. 20 (2019) 100701, https://doi.org/10.1016/j.nme.2019.100701.

[12] K. Wang, H. Sun, X. Zan, U.M. Ciucani, W. Pantleon, L. Luo, Y. Wu, Evolution of microstructure and texture of moderately warm-rolled pure tungsten during annealing at 1300 °C, J. Nucl. Mater. 540 (2020), 152412, https://doi.org/10.1016/j.jnucmat.2020.152412.

[13] M. Fukuda, A. Hasegawa, T. Tanno, S. Nogami, H. Kurishita, Property change of advanced tungsten alloys due to neutron irradiation, J. Nucl. Mater. 442 (2013) S273–S276, https://doi.org/10.1016/j.jnucmat.2013.03.058.

[14] G. Pintsuk, I. Bobin-Vastra, S. Constans, P. Gavila, M. Rödig, B. Riccardi, Qualification and post-mortem characterization of tungsten mock-ups exposed to cyclic high heat flux loading, Fusion Eng. Des. 88 (2013) 1858–1861, https://doi.org/10.1016/j.fusengdes.2013.05.091.

[15] V. Shah, J.A.W. van Dommelen, S.E.S. Heijkoop, M.A. Oude Vrielink, M.G.D. Geers, A numerical model for the recrystallization kinetics of tungsten monoblocks under cyclic heat loads, Fusion Eng. Des. 173 (2021), 112827, https://doi.org/10.1016/j.fusengdes.2021.112827.

[16] S. Antusch, E. Visca, A. Klein, H. Walter, K. Pursche, M. Wirtz, T. Loewenhoff, H. Greuner, B. Böswirth, J. Hoffmann, D. Bolich, G. Pintsuk, M. Rieth, Manufacturing, high heat flux testing and post mortem analyses of a W-PIM mock-up, Nucl. Mater. Energy. 20 (2019), 100688, https://doi.org/10.1016/j.nme.2019.100688.

[17] J.H. You, E. Visca, T. Barrett, B. Böswirth, F. Crescenzi, F. Domptail, M. Fursdon, F. Gallay, B.E. Ghidersa, H. Greuner, M. Li, A.V. Müller, J. Reiser, M. Richou, S. Roccella, C. Vorpahl, European divertor target concepts for DEMO: Design rationales and high heat flux performance, Nucl. Mater. Energy. 16 (2018) 1–11, https://doi.org/10.1016/j.nme.2018.05.012.

[18] E. Visca, S. Libera, A. Mancini, G. Mazzone, A. Pizzuto, C. Testani, Hot radial pressing: An alternative technique for the manufacturing of plasma-facing components, Fusion Eng. Des. 75–79 (2005) 485–489, https://doi.org/10.1016/j.fusengdes.2005.06.123.

[20] H. Greuner, B. Boeswirth, J. Boscary, P. McNeely, High heat flux facility GLADIS: Operational characteristics and results of W7-X pre-series target tests, J. Nucl. Mater. 367–370 B (2007) 1444–1448, https://doi.org/10.1016/j.jnucmat.2007.04.004.

[21] H. Greuner, B. Böswirth, K. Hunger, A. Khan, T.R. Barrett, F. Gallay, M. Richou, E. Visca, A.V. Müller, J.H. You, Assessment of the high heat flux performance of European DEMO divertor mock-ups, Phys. Scr. 2020 (2020), https://doi.org/10.1088/1402-4896/ab3681.

[23] Kuo Zhang, Jeong-Ha You, Crack formation in the tungsten armour of divertor targets under high heat loads: A computational fracture mechanics study, Fusion Eng. Des. (184) (2022) 113305, https://doi.org/10.1016/j.fusengdes.2022.113305.

[24] P. Gavila, B. Riccardi, G. Pintsuk, G. Ritz, V. Kuznetsov, A. Durocher, High heat flux testing of EU tungsten monoblock mock-ups for the ITER divertor, Fusion Eng. Des. 98–99 (2015) 1305–1309, https://doi.org/10.1016/j.fusengdes.2014.12.006.

[25] A. Manhard, Deuterium inventory in tungsten after plasma exposure: a microstructural survey, Universität Augsburg, 2011. PhD Thesis.

[26] J.H. You, M. Li, K. Zhang, Structural lifetime assessment for the DEMO divertor targets: Design-by-analysis approach and outstanding issues, Fusion Eng. Des. 164 (2021), 112203, https://doi.org/10.1016/j.fusengdes.2020.112203.

[27] M. Monz, P. Hudleston, D. Prior, Z. Michels, S. Fan, M. Negrini, P. Langhorne, C. Qi, Electron backscatter diffraction (EBSD) based determination of crystallographic preferred orientation (CPO) in warm, coarse-grained ice: a case study, Storglaciären, Sweden, Cryosph. Discuss. (2020) 1–24.

[28] Y. Yuan, J. Du, M. Wirtz, G.N. Luo, G.H. Lu, W. Liu, Surface damage and structure evolution of recrystallized tungsten exposed to ELM-like transient loads, Nucl. Fusion. 56 (2016), https://doi.org/10.1088/0029-5515/56/3/036021.

[29] A. Alfonso, D. Juul Jensen, G.N. Luo, W. Pantleon, Thermal stability of a highly-deformed warm-rolled tungsten plate in the temperature range 1100-1250 °c, Fusion Eng. Des. 98–99 (2015) 1924–1928, https://doi.org/10.1016/j.fusengdes.2015.05.043.

[30] M. Wirtz, G. Cempura, J. Linke, G. Pintsuk, I. Uytdenhouwen, Thermal shock response of deformed and recrystallised tungsten, Fusion Eng. Des. 88 (2013) 1768–1772, https://doi.org/10.1016/j.fusengdes.2013.05.077.

[31] V. Shah, J.A.W. van Dommelen, E. Altstadt, A. Das, M.G.D. Geers, Brittle-ductile transition temperature of recrystallized tungsten following exposure to fusion relevant cyclic high heat load, J. Nucl. Mater. 541 (2020), https://doi.org/10.1016/j.jnucmat.2020.152416.

[32] V. Shah, J.T.S. Beune, Y. Li, T. Loewenhoff, M. Wirtz, T.W. Morgan, J.A.W. van Dommelen, Recrystallization behaviour of high-flux hydrogen plasma exposed tungsten, J. Nucl. Mater. 545 (2021), https://doi.org/10.1016/j.jnucmat.2020.152748.

[33] F. Crescenzi, C. Bonnekoh, S. Roccella, E. Visca, J.H. You, ITER-like divertor target for DEMO: Design study and fabrication test, Fusion Eng. Des. 124 (2017) 432–436, https://doi.org/10.1016/j.fusengdes.2017.02.014.

[34] J.A.R. Saad, Tungsten Recrystallization Behaviour Under Steady and Transient Hydrogen Plasma Loading, (2018) Thesis.

[35] I. Gutierrez-Urrutia, S. Zaefferer, D. Raabe, Electron channeling contrast imaging of twins and dislocations in twinning-induced plasticity steels under controlled diffraction conditions in a scanning electron microscope, Scr. Mater. 61 (2009) 737–740, https://doi.org/10.1016/j.scriptamat.2009.06.018.

[36] G. Pintsuk, S. Antusch, T. Weingaertner, M. Wirtz, Recrystallization and composition dependent thermal fatigue response of different tungsten grades, Int. J. Refract. Met. Hard Mater. 72 (2018) 97–103, https://doi.org/10.1016/j.ijrmhm.2017.11.039.